Int. J. Electrochem. Sci., 17 **(2022)** Article Number: 2212106, doi: 10.20964/2022.12.97

International Journal of
ELECTROCHEMICAL
SCIENCE
www.electrochemsci.org

Short Communication

Electrical Resistance Sensor Based on ZnO Nanoarray for VOC Gas Detection

Hua Tian[1,*], *Zhigang Wu*[2]

[1] Chemical Engineering Institute, Northwest Minzu University, Gansu, Lanzhou, 730030, China
[2] CSCEC AECOM Consultants CO., Ltd. Gansu, Lanzhou, 730030, China
[*]E-mail: sarahmimi1115@sina.com

Received: 28 October 2022 / *Accepted:* 24 November 2022 / *Published:* 27 December 2022

Volatile Organic Compounds (VOCs) are widely present in our daily environment. Due to its larger tunable space and better structural properties, ZnO has been widely used in the field of optical and electrical sensing in recent years, especially in the field of gas-sensitive sensing, which has excellent research prospects. In this work, ZnO arrays were prepared and their gas-sensitive sensing performance for formaldehyde gas was systematically investigated. It is found that the ZnO array gas sensing element has better sensing performance compared with the reference sample, and the increase of hole size contributes to the improvement of sensitivity. The lower detection limit of the optimal gas sensing element for formaldehyde gas can reach 10 ppb, which is much lower than the national requirement (60 ppb). The detection performance of the ZnO array for VOC acetone was also measured.

Keywords: ZnO array; VOC; Methylene blue; Electrochemical properties; Cardiovascular

1. INTRODUCTION

With the development of science and technology and industrial technology, gasoline, rubber, pesticides, plastic products and other products bring great convenience to mankind, but at the same time in its production process will produce some gases that are harmful to human health and the environment [1–4]. Volatile organic compounds (VOCs) are one of the most important of these hazardous gases. With the passage of time and human neglect, the environmental pollution problems caused by them have become increasingly serious. Secondary pollutants produced by photochemical reactions of VOCs in the atmosphere when exposed to ultraviolet light can lead to higher concentrations of PM10 and O3, forming hazy weather [5,6]. At the same time, VOCs emissions from some household and construction materials can simultaneously form pollution indoors and affect people's health. In order to improve the quality of ambient air, it is imperative to detect VOCs in the environment [7,8].

In general, VOCs are volatile organic compounds with a boiling point between 50°C and 260°C and a saturated vapor pressure of more than 133.322 kPa at room temperature. Its main components are hydrocarbons, oxygen hydrocarbons, halogenated hydrocarbons, nitrogen hydrocarbons and sulfur hydrocarbons, low boiling point polycyclic aromatic hydrocarbons [9–12]. It is a class of organic pollutants that are commonly found in the air and have a complex composition. The chemical properties carried by them show a certain degree of toxicity, irritation, and may have a carcinogenic effect, resulting in a variety of discomfort symptoms after inhalation [13]. At present, more than 300 kinds of volatile organic compounds can be identified, according to the different chemical structures [14], VOCs can be divided into five categories: non-methane hydrocarbons (alkanes, alkenes, alkynes, aromatic hydrocarbons), halogenated hydrocarbons, oxygen-containing organic compounds (alcohols, aldehydes, ketones, phenols, ethers, acids, esters, etc.), nitrogen-containing organic compounds (amines, cyanides, etc.) and sulfur-containing organic compounds [15–19].

There are many technical methods for the detection and analysis of VOCs, mainly gas chromatography (GC), gas chromatography-mass spectrometry (GC-MS), high performance liquid chromatography (HPLC), fluorescence photometry, pulse discharge detector method and other methods. Among them, GC and GC-MS are the two more commonly used methods [20–26]. In addition, the colorimetric tube detection method can provide a rough but rapid detection of VOCs. The electrochemical gas sensor detection method uses the electrolytic current generated by the reaction of a gas with an electrolyte solution as the sensor output, which yields the gas concentration [27–30]. Seknar et al.[31] used the pulse discharge technique (PDT) signal modulation method in order to improve the sensitivity of electrochemical gas sensors to methane. Menar [32] developed a new formaldehyde gas sensor using a carbon electrode as a substrate with a polyacrylate hydrazine attached for accumulating formaldehyde and converting it to hydrazone.

ZnO is a group II-VI compound semiconductor material. Due to the wide band gap, at room temperature, pure ZnO in ideal chemical ratios is an insulator and not a semiconductor. However, the actual ZnO single crystals are N-type semiconductors [33], which are caused by intrinsic ZnO point defects (zinc gap-filling atoms or oxygen vacancies). Due to these intrinsic defects, the ZnO chemical ratios are non-idealized, resulting in carrier concentrations that can vary over a wide range (up to 10 orders of magnitude) [34]. ZnO is a gas-sensitive material, and the doping elements in it have a great influence on the gas-sensitive performance. After some elements doping can have good sensitivity to organic vapor, combustible gas, harmful gas and can be used to make a variety of gas-sensitive sensor devices [35,36]. In this work, we used $Zn(NO_3)_2$ and $(CH_2)_6N_4$ as the mixed reaction solution to synthesize ZnO nanoarrays using a simple water bath method. The gas-sensitive properties of ZnO nanoarrays were systematically investigated for the room VOC gases formaldehyde and acetone.

2. EXPERIMENTAL

2.1. Chemicals

$Zn(NO_3)_2{\cdot}6H_2O$, $Zn(CH_3COO)_2{\cdot}2H_2O$, $(CH_2)_6N_4$ was purchased from Xilong Chemical Co. NaOH, $C_6H_5O_7Na_3{\cdot}2H_2O$, $H_2C_2O_4$, CH_3CH_2OH and CH_3COCH_3 were purchased from Beijing Chemical Plant. Si(100) was acquired from Shenzhen Southern Glass Group.

2.2. Preparation of precursor solution

A certain amount of zinc nitrate hexahydrate ($Zn(NO_3)_2 \cdot 6H_2O$) was weighed and put into 100ml beaker A, and deionized water was added to fully dissolve it. Weigh a certain amount of hexamethylenetetramine ($(CH_2)_6N_4$) into 100 mL beaker B and add deionized water to dissolve it fully. The zinc nitrate solution from beaker A is diverted into the hexamethylenetetramine solution in beaker B with a glass rod to mix well.

2.3. ZnO array preparation

A silicon wafer with a flat and smooth surface is selected as the substrate, and metallic zinc is thermally vaporized on the wafer and passed through high temperature oxygen to react to form a thin film of zinc oxide (the thickness of the film is 45 nm). After the substrate is cooled, a layer of photoresist with a thickness of 45 nm is sprayed on the film. Then local electron beam exposure is performed on the photoresist to obtain an array of holes with an average pore size of 300 nm. Prepare a certain concentration of zinc nitrate and hexamethylenetetramine solution, mix and stir for 30 min. The treated wafers were put into the above solution and reacted at 95°C for 3 h. After removal, the wafers were rinsed several times with deionized water and dried to obtain ZnO nanostructured materials on the wafers. Hydrothermally synthesized normal ZnO nanomaterials were also used as a comparison (denoted as ZnO NPs). The ZnO arrays denoted as ZnO-A1 before annealing. The ZnO arrays denoted as ZnO-A2 after annealing.

2.4. Sensor preparation

The specific process of gas-sensitive element preparation is divided into the following steps: (1) The prepared ZnO array is carefully scraped off with a small knife. (2) The scraped ZnO arrays were collected and dispersed into a certain amount of anhydrous ethanol with a sample to binder weight ratio of about 5:1, ground and blended into a homogeneous paste. (3) Using a very fine brush, the paste-like sample is evenly coated onto the ceramic tube electrode with two pairs of gold electrodes, where the coating standard requires the sample thickness to be about 0.25 mm, and the sample should cover all the electrodes evenly and continuously. (4) After waiting for the complete evaporation of the binder, the resulting ceramic tube electrodes covered with ZnO arrays were thermally annealed (400°C) for 2 h. (5) A spring-like heating wire of Ni-Cr alloy is carefully inserted into the prepared ceramic tube coated with ZnO array. (6) Solder the prepared ceramic tube electrode pins to the sample base along with the heating wire pins. (7) The soldered sample base is inserted into the test board and placed on the aging table. The board is then aged at an aging voltage of 5 V for 6 days.

2.5. Gas sensitive testing of sensors

The gas-sensitive characteristics of gas-sensitive components are measured with the Model WS-30A Gas-Sensitive Component Test System (Zhengzhou Weisheng Co., Ltd., China). The test voltage

remains constant at 5V during the entire test of the gas sensitivity. The target test gases used during the measurement are prepared from 1000 ppm standard gases using the static gas distribution method. First, the target test gas and gases such as nitrogen and oxygen are injected into the evacuated gas chamber (chamber size 18L). Then, the gas in the chamber is mixed with clean ambient air, and the oxygen content and humidity of the mixed gas components are required to be 21% and 10%, respectively. The gas sensing element to be tested is then placed in the mixed target test gas of various volume fractions. After the response value of the gas sensing element has stabilized, the gas sensing element is removed from the test gas and placed back in the ambient air until the element returns to its initial state.

The sensitivity of a gas-sensitive element is determined by the ratio of the resistance of the gas-sensitive element in air and in the target test gas. Since ZnO is an n-type semiconductor oxide, the sensitivity of the gas sensing element is defined as Response= Ra/Rg. Where Ra and Rg represent the resistance of the gas-sensitive element in air and in the target test gas, respectively. Response time is defined as the time it takes for the resistance value to change from Ra to 90% of the difference between Rg and Ra when the gas sensing element is placed in the gas being measured. Conversely, the recovery time is defined as the time it takes for the gas sensing element to recover from Rg to 90% of Ra to Rg when it is removed from the gas being measured and placed back in ambient air.

3. RESULTS AND DISCUSSION

The crystal structure and orientation of the samples were analyzed by XRD. Figure 1A shows the XRD patterns of the ZnO nanopowders prepared using hydrothermal synthesis. Upon comparison with the JCPDS standard card (JCPDS36-1451) for ZnO, it can be seen that Figure 1A is in perfect agreement with the standard spectrum of ZnO. Figure 1B shows the XRD pattern of the product obtained after hydrothermal growth at 90 degrees for 3 h on a ZnO coated wafer substrate under a certain growth environment [37–39]. From Fig. 1B, three strong peaks appear at 2θ = 31.55°, 34.34°, and 36.18°, corresponding to the crystallographic indices (100), (002), and (101), respectively, which are fully consistent with the JCPDS card standard (JCPDS36-1451). However, the polar plane of the hexagonal crystal system does not appear as the strongest diffraction peak, which indicates that there is no tendency for the fabricated product to grow selectively [40,41]. At the same time, the diffraction peaks of Si inevitably appear when Si sheets are used as the substrate. Figure 1C shows the XRD patterns of the ZnO nanoarrays prepared under hydrothermal growth conditions and heat treated at 800 °C. As seen from the figure, a clear strong peak appears at 2θ= 34.34°, i.e., a relatively high diffraction peak in the (002) plane [42]. This indicates that the ZnO nanoarrays grown on Si sheets with ZnO crystalline species attached have been heat-treated at high temperature and have the characteristics of selective orientation along the (002) crystal plane [43,44]. The diffraction peak of SiO appears at 2θ=58.98°, indicating that the Si substrate also undergoes oxidation reaction to generate new phases after heat treatment.

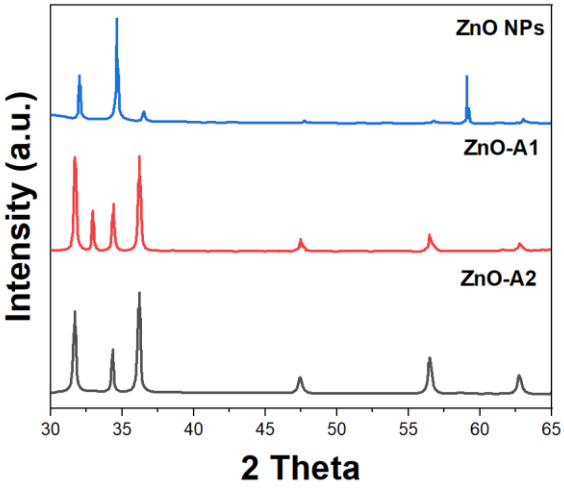

Figure 1. XRD patterns of (A) ZnO NPs (B) ZnO-A1 and (C) ZnO-A2.

Figure 2 shows the nitrogen sorption-desorption isotherm of the sample, where the inset is the corresponding pore size distribution curve. The adsorption-desorption isotherms obtained from the sample tests can be judged according to the IUPAC classification. Both the ZnO and ZnO arrays prepared by direct hydrothermal method exhibited Type-IV isotherms before heat treatment, and the isotherms showed capillary condensation at relative pressures (P/P_0) between 0.4 and 0.8. This confirms the presence of mesopores in the sample structure [45]. The specific surface area and major pore size distributions of ZnO, ZnO arrays before and after heat treatment were 24.2 m^2/g (9.3 nm), 46.7 m^2/g (7.4 nm) and 55.7 m^2/g (9.3 nm), respectively. It is well known that during annealing of metal-semiconductor oxides primary particles aggregate to form secondary particles, which in turn lead to the formation of a large number of mesoporous structures [46]. In summary, it is clear that the gas sensing film prepared in this work is a macroporous structured ZnO array with a sub-porous structure.

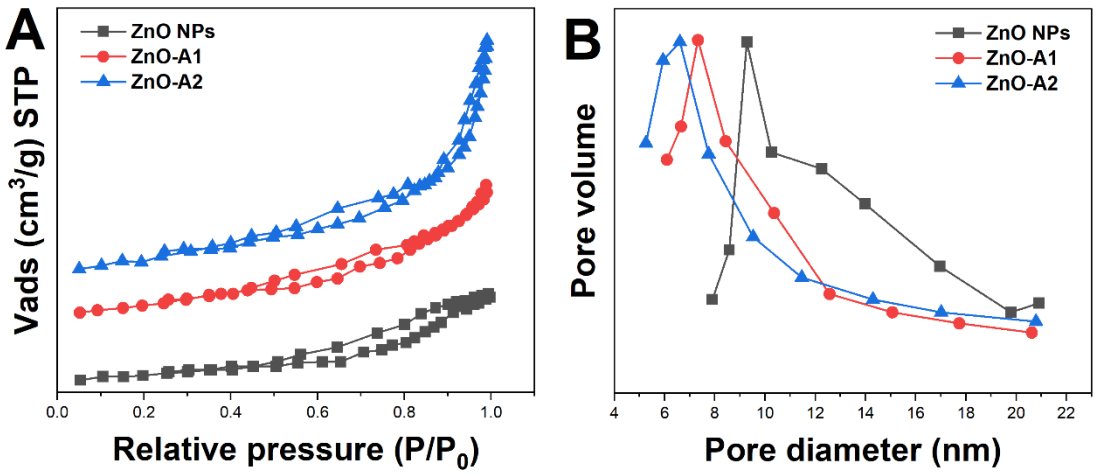

Figure 2. Adsorption–desorption isotherm and BJH pore–size distribution plots (A) ZnO NPs (B) ZnO-A1 and (C) ZnO-A2.

Figure 3 compares the sensitivity of the ZnO gas sensing element for 100 ppm formaldehyde gas with the operating temperature curve. As shown in the figure, all gas sensing elements exhibit typical N-type semiconductor oxide gas sensor characteristics [47,48]. The gas-sensitive element becomes less resistive after exposure to the reducing gas formaldehyde. The relationship between sensitivity and temperature for all gas-sensitive elements showed the same trend [49]. When the temperature is relatively low, the response value of the gas-sensitive element gradually increases as the temperature continues to increase until it reaches its maximum response value [50]. Subsequently, as the temperature continues to increase, the response value of the gas-sensitive element decreases [51]. It can also be observed from the figure that the sensitivity of both ZnO-A1 and ZnO-A2 is significantly enhanced compared to that of ZnO NPs. The sensitivity of ZnO NPs, ZnO-A1 and ZnO-A2 were 18, 274 and 629 at the optimum operating temperature of 215°C, respectively.

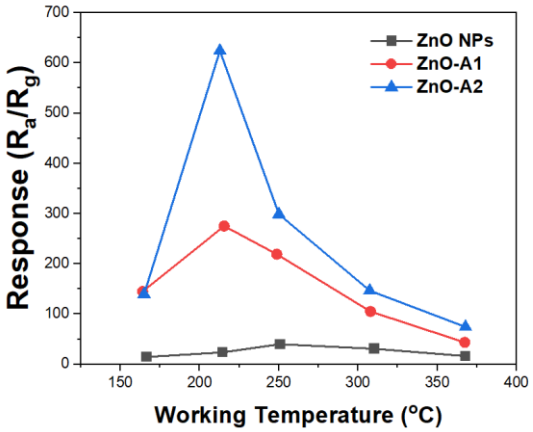

Figure 3. Responses of ZnO NPs, ZnO-A1 and ZnO-A2 towards 100 ppm formaldehyde.

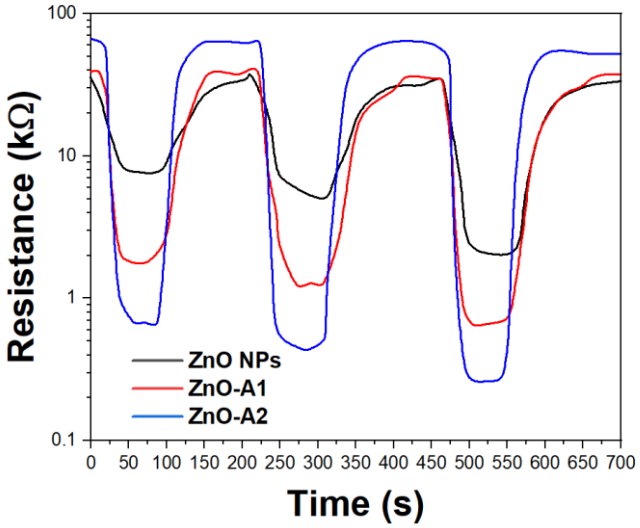

Figure 4. Transient response of ZnO NPs, ZnO-A1 and ZnO-A2 to 3-300 ppm formaldehyde at 215°C.

Figure 4 records the response and recovery dynamics of ZnO NPs, ZnO-A1 and ZnO-A2 gas sensing elements at 215°C for 30, 50 and 100 ppm formaldehyde gas, respectively. As shown in the figure, the response values of all gas-sensitive elements increase sharply with the introduction of formaldehyde gas [52]. When the formaldehyde gas is evacuated and the gas sensing element is placed in ambient air again, the gas sensing element returns to its initial state. This indicates that the gas-sensitive element has a fast and repeatable response to formaldehyde gas. The response/recovery times of the ZnO NPs, ZnO-A1 and ZnO-A2 gas sensing elements for 100 ppm formaldehyde gas were calculated to be 14s/140s, 14s/76s and 12s/58s, respectively. In oxidizing gases, the electron affinity of the adsorbed gas is greater than the work function of the semiconductor. Electrons will be transferred from semiconductor to gas, and the gas will be absorbed by a negative charge in the form of a negative charge. In this case, the semiconductor loses the electronic surface band and bends upward, increasing the surface resistance. In a reducing gas, the electron affinity of the adsorbed gas is less than the work function of the semiconductor. Electrons will be transferred from the gas to the semiconductor, and the gas will lose the electrons and attach to the semiconductor surface as a positive charge. In this case, the number of electrons in the semiconductor conductor band increases and the semiconductor resistance decreases .In this work, we specially prepared a kind of array sensing material. Due to the uniform and excellent adsorption performance of ZnO array, this sensor can be very sensitive to VOC detection.

The dependence between the sensitivity values of ZnO NPs, ZnO-A1 and ZnO-A2 gas sensing elements and the concentration of formaldehyde gas is shown in Figure 5A. We are able to see from the graph that the response value of the gas sensing element has a good linear relationship with the formaldehyde gas concentration in the range of 3-300 ppm. The slopes of the fitted straight lines for ZnO NPs, ZnO-A1 and ZnO-A2 were calculated to be 0.30 ,1.21 and 7.2, respectively. This indicates a positive correlation between the large pore size and the sensitivity value of formaldehyde gas. The sensitivity values of the ZnO-A1 and ZnO-A2 gas sensing elements are positively and linearly related to the formaldehyde gas concentration. It should be noted that the sensitivity curve of the ZnO NPs gas sensing element versus the concentration of formaldehyde gas is not given in the figure because the signal-to-noise ratio of the ZnO NPs gas sensing element is relatively high and cannot distinguish formaldehyde gas at ultra-low concentrations in a gradient [53]. As shown in Figure 5B, the sensitivity of the ZnO-A2 gas-sensitive element is the highest. The sensitivity range is 2-32 when detecting formaldehyde gas in the concentration range of 0.01-3 ppm. In addition, the response signals of the ZnO-A1 and ZnO-A2 gas sensing elements can be visualized even at a detection concentration of 10 ppb. When $Ra/Rg \geq 1.2$ is defined as the theoretical lower detection limit of the gas sensing element, it is calculated that the lowest detection limits of ZnO-A1 and ZnO-A2 gas sensing elements can reach 8.5 and 2.51 ppb, respectively. Table 1 shows the comparison of the proposed gas sensor with previous reports.

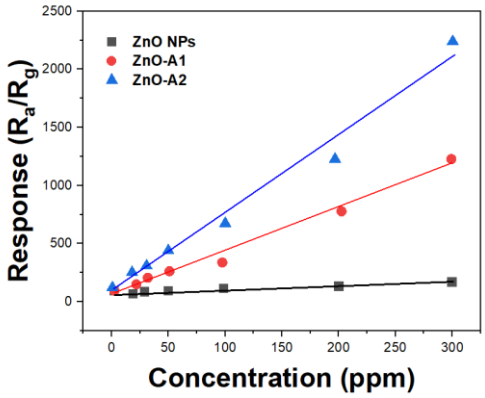

Figure 5. (A) Response curves of ZnO NPs, ZnO-A1 and ZnO-A2 towards to 3-300 ppm formaldehyde gas at 215°C.

Table 1. Sensing performances of ZnO gas sensors reported in literatures to VOCs.

Material	Gas	LOD (ppm)	Reference
Pd@Co_3O_4-ZnO nanofibers	Formaldehyde	1	[54]
Au/F-ZnO	Ethanol	5	[55]
ZnO/$ZnFe_2O_4$ hollow nanocages	Acetone	1	[56]
Hierarchical ZnO spheres	Acetone	0.25	[57]
ZnO-A2	Formaldehyde	0.00251	This work

Figure 6 shows the gas sensitive sensitivity response values of ZnO NPs, ZNO-A1 and ZNO-A2 gas sensitive elements to 50 ppm acetone gas at different operating temperatures. As can be seen from the figure, all the gas sensitive elements exhibit typical N-type semiconductor gas sensitive elements characteristics, and no gas sensitive elements exhibit P-type semiconductor gas sensitive elements characteristics. By observing the curves in Figure 6, it can be seen that all the relation curves showed an increasing trend of sensitivity with the increase of temperature until reaching the maximum value. Subsequently, the sensitivity decreases with increasing temperature. When the operating temperature is relatively low, the number of active sites on the surface of the gas sensitive element is limited, so that the reaction between the target gas acetone gas and the active sites on the surface of the gas sensitive element is not complete [58]. With the increase of working temperature, the number of active sites on the surface of the gas sensor increases, and the degree of reaction between acetone gas and active sites continues to strengthen. However, if the working temperature continues to increase, the desorption degree of the gas on the surface of the gas sensitive element may be greater than the adsorption degree, which will lead to the reduction of the gas sensitive sensitivity of the gas sensitive element.

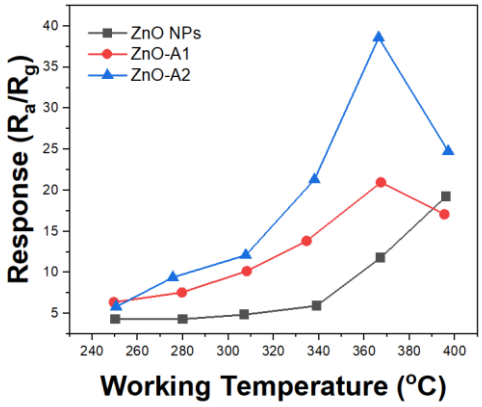

Figure 6. Responses of ZnO NPs, ZnO-A1 and ZnO-A2 towards 50 ppm acetone.

The dynamic curves in FIigure 7 record in detail the response and recovery dynamic curves of ZnO NPs, ZNO-A1 and ZNO-A2 gas sensitive elements within a complete cycle when the operating temperature is 370°C and the detection target gas acetone concentration is 50 ppm. As can be seen from the dynamic recording curve in the figure, when the gas sensitive element placed in the ambient air contacts the target gas acetone, the response values of all gas sensitive elements increase sharply until reaching a stable value. Subsequently, when acetone gas was removed and the gas sensitive elements were replaced in ambient air, the response values of all gas sensitive elements decreased and quickly returned to their initial state. By comparing the dynamic response curve in Figure 7 with the curve in Figure 6, it can be found that the sensitivity of each gas sensitive element has the same trend.

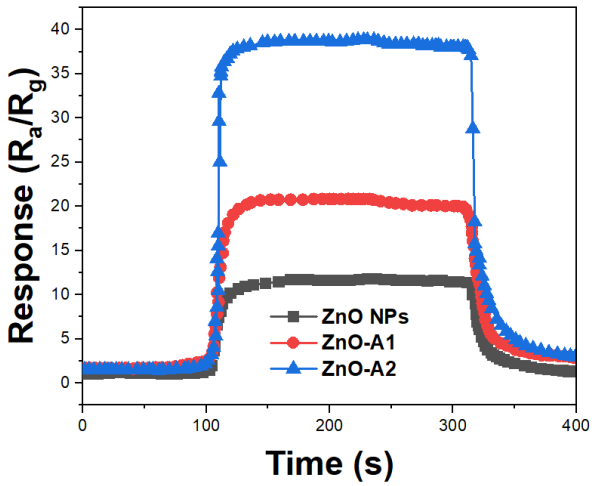

Figure 7. One circle dynamic response of ZnO NPs, ZnO-A1 and ZnO-A2 sensors to 50 ppm of acetone under 370°C.

4. CONCLUSION

The main factor affecting the gas-sensitive performance of gas sensors is the sensitive material used to prepare the gas-sensitive element, and the morphology and dimensional structure of the sensitive material largely determine the physical properties of the material. Structurally, the unique array structure of ZnO provides a large pore capacity and a large specific surface area, which provides an ideal platform for studying the surface state and surface reactions of materials. In terms of performance, the ZnO array helps to enhance the gas-sensitive performance of the gas-sensitive element. The results demonstrate that the ZnO array does not change the optimal operating temperature of the gas-sensitive element, but has significant benefits in enhancing the sensitivity of the gas-sensitive element. The large hole size leads to an increase in gas sensitivity of the gas sensing element. The optimal gas-sensitive element in the work, ZnO-A2, shows an approximately 35-fold increase in sensitivity compared to the reference sample, while exhibiting better gas sensitivity selectivity and stability.

ACKNOWLEDGEMENTS
This work was supported by the Fundamental Research Funds for the Central Universities (No. 31920180081).

References

1. M. Ghazi, S. Janfaza, H. Tahmooressi, N. Tasnim, M. Hoorfar, *Journal of Hazardous Materials*, 424 (2022) 127566.
2. L. Vigna, A. Verna, S.L. Marasso, M. Sangermano, P. D'Angelo, F.C. Pirri, M. Cocuzza, *Sensors and Actuators B: Chemical*, 345 (2021) 130381.
3. F. Yin, W. Yue, Y. Li, S. Gao, C. Zhang, H. Kan, H. Niu, W. Wang, Y. Guo, *Carbon*, 180 (2021) 274–297.
4. J. Lu, M. Cheng, C. Zhao, B. Li, H. Peng, Y. Zhang, Q. Shao, M. Hassan, *Industrial Crops and Products*, 176 (2022) 114267.
5. X. Chen, K.G. Muhammad, C. Madeeha, W. Fu, L. Xu, Y. Hu, J. Liu, K. Ying, L. Chen, G.O. Yurievna, *Lung Cancer*, 154 (2021) 197–205.
6. D. Li, G. Liu, Q. Zhang, M. Qu, Y.Q. Fu, Q. Liu, J. Xie, *Sensors and Actuators B: Chemical*, 331 (2021) 129414.
7. F. Kus, C. Altinkok, E. Zayim, S. Erdemir, C. Tasaltin, I. Gurol, *Sensors and Actuators B: Chemical*, 330 (2021) 129402.
8. M. Fois, T. Cox, N. Ratcliffe, B. de Lacy Costello, *Sensors and Actuators B: Chemical*, 330 (2021) 129264.
9. S.M. Aghaei, A. Aasi, S. Farhangdoust, B. Panchapakesan, *Applied Surface Science*, 536 (2021) 147756.
10. E. Daulton, A.N. Wicaksono, A. Tiele, H.M. Kocher, S. Debernardi, T. Crnogorac-Jurcevic, J.A. Covington, *Talanta*, 221 (2021) 121604.
11. T. Kuchmenko, R. Umarkhanov, L. Lvova, *Sensors and Actuators B: Chemical*, 322 (2020) 128585.
12. S. Khan, S. Le Calvé, D. Newport, *Sensors and Actuators A: Physical*, 302 (2020) 111782.
13. A. Di Gilio, A. Catino, A. Lombardi, J. Palmisani, L. Facchini, T. Mongelli, N. Varesano, R. Bellotti, D. Galetta, G. de Gennaro, *Cancers*, 12 (2020) 1262.

14. S. Zeinali, S. Homayoonnia, G. Homayoonnia, *Sensors and Actuators B: Chemical*, 278 (2019) 153–164.
15. M.R. Miah, M. Yang, S. Khandaker, M.M. Bashar, A.K.D. Alsukaibi, H.M.A. Hassan, H. Znad, Md.R. Awual, *Sensors and Actuators A: Physical*, 347 (2022) 113933.
16. B. Li, X. Zhang, L. Huo, S. Gao, C. Guo, Y. Zhang, Z. Major, F. Zhang, X. Cheng, Y. Xu, *Journal of Hazardous Materials*, 435 (2022) 129005.
17. A. D'Arco, T. Mancini, M.C. Paolozzi, S. Macis, L. Mosesso, A. Marcelli, M. Petrarca, F. Radica, G. Tranfo, S. Lupi, *Sensors*, 22 (2022) 5624.
18. P.P. Conti, R.S. Andre, L.A. Mercante, L. Fugikawa-Santos, D.S. Correa, *Sensors and Actuators B: Chemical*, 344 (2021) 130124.
19. D. Kuang, L. Wang, X. Guo, Y. She, B. Du, C. Liang, W. Qu, X. Sun, Z. Wu, W. Hu, Y. He, *Journal of Hazardous Materials*, 416 (2021) 126171.
20. W. Shi, X. Huo, Y. Tian, X. Lu, L. Yang, Q. Zhou, X. Wang, Q. Yu, *Talanta*, 230 (2021) 122352.
21. H. Li, X. Kang, S. Wang, H. Mo, D. Xu, W. Zhou, L. Hu, *Food Control*, 121 (2021) 107636.
22. C. Lai, Z. Wang, L. Qin, Y. Fu, B. Li, M. Zhang, S. Liu, L. Li, H. Yi, X. Liu, X. Zhou, N. An, Z. An, X. Shi, C. Feng, *Coordination Chemistry Reviews*, 427 (2021) 213565.
23. R.L. Pérez, C.E. Ayala, J.-Y. Park, J.-W. Choi, I.M. Warner, *Chemosensors*, 9 (2021) 153.
24. L. Feng, C. Dong, M. Li, L. Li, X. Jiang, R. Gao, R. Wang, L. Zhang, Z. Ning, D. Gao, J. Bi, *Journal of Hazardous Materials*, 388 (2020) 121816.
25. C. Megías-Sayago, I. Lara-Ibeas, Q. Wang, S. Le Calvé, B. Louis, *Journal of Environmental Chemical Engineering*, 8 (2020) 103724.
26. B. Li, Q. Zhou, S. Peng, Y. Liao, *Frontiers in Chemistry*, 8 (2020) 321.
27. J. Ke, S. Li, D. Zhao, *Journal of the Air & Waste Management Association*, 70 (2020) 862–875.
28. B.P. Chandra, C.D. McClure, J. Mulligan, D.A. Jaffe, *Atmosphere*, 11 (2020) 276.
29. S. Acharyya, S. Nag, P.K. Guha, *IEEE Sensors Journal*, 21 (2020) 5771–5778.
30. Y. Bao, P. Xu, S. Cai, H. Yu, X. Li, *Talanta*, 182 (2018) 148–155.
31. P.K. Sekhar, J. Kysar, E.L. Brosha, C.R. Kreller, *Sensors and Actuators B: Chemical*, 228 (2016) 162–167.
32. M.E. Pacheco, C.B. Castells, L. Bruzzone, *Sensors and Actuators B: Chemical*, 238 (2017) 660–666.
33. N. Al-Hardan, M. Abdullah, A.A. Aziz, H. Ahmad, L. Low, *Vacuum*, 85 (2010) 101–106.
34. N. Kaur, D. Zappa, M. Ferroni, N. Poli, M. Campanini, R. Negrea, E. Comini, *Sensors and Actuators B: Chemical*, 262 (2018) 477–485.
35. N. Kilinc, O. Cakmak, A. Kosemen, E. Ermek, S. Ozturk, Y. Yerli, Z.Z. Ozturk, H. Urey, *Sensors and Actuators B: Chemical*, 202 (2014) 357–364.
36. F. Xu, C. Zhou, H.-P. Ho, *Journal of Alloys and Compounds*, 858 (2021) 158294.
37. A.G. Acedo-Mendoza, A. Infantes-Molina, D. Vargas-Hernández, C.A. Chávez-Sánchez, E. Rodríguez-Castellón, J.C. Tánori-Córdova, *Materials Science in Semiconductor Processing*, 119 (2020) 105257.
38. Y. Caglar, M. Caglar, S. Ilican, *Optik*, 164 (2018) 424–432.
39. E. Doustkhah, M. Esmat, N. Fukata, Y. Ide, D.A.H. Hanaor, M.H.N. Assadi, *Chemosphere*, 303 (2022) 134932.
40. N. Fathima, N. Pradeep, J. Balakrishnan, *Materials Science in Semiconductor Processing*, 90 (2019) 26–31.
41. Y. Jing, H. Yin, C. Li, J. Chen, S. Wu, H. Liu, L. Xie, Q. Lei, M. Sun, S. Yu, *Environmental Research*, 203 (2022) 111819.
42. N.R. Khalid, A. Hammad, M.B. Tahir, M. Rafique, T. Iqbal, G. Nabi, M.K. Hussain, *Ceramics International*, 45 (2019) 21430–21435.
43. S.K. Mandal, K. Dutta, S. Pal, S. Mandal, A. Naskar, P.K. Pal, T.S. Bhattacharya, A. Singha, R. Saikh, S. De, D. Jana, *Materials Chemistry and Physics*, 223 (2019) 456–465.

44. S. Kumar, R.D. Kaushik, G.K. Upadhyay, L.P. Purohit, *Journal of Hazardous Materials*, 406 (2021) 124300.
45. A.A. Menazea, N.S. Awwad, *Journal of Materials Research and Technology*, 9 (2020) 9434–9441.
46. O. URPER, N. BAYDOGAN, *Materials Letters*, 274 (2020) 128000.
47. K. Lee, D.-H. Baek, J. Choi, J. Kim, *Sensors and Actuators B: Chemical*, 264 (2018) 249–254.
48. Y. Luo, A. Ly, D. Lahem, J.D.M. Martin, A.-C. Romain, C. Zhang, M. Debliquy, *Sensors and Actuators B: Chemical*, 360 (2022) 131674.
49. G. Marappan, K. Pushparaj, Y. Sivalingam, V. Nutalapati, V.J. Surya, *Materials Letters*, 304 (2021) 130724.
50. N. Naseri, S. Kharrazi, K. Abdi, R. Alizadeh, *Analytica Chimica Acta*, 1183 (2021) 338983.
51. T.N.T. Oliveira, T.M. Perfecto, C.A. Zito, D.P. Volanti, *Sensors and Actuators Reports*, 3 (2021) 100064.
52. M. Salimi, S.M.R. Milani Hosseini, *Sensors and Actuators B: Chemical*, 344 (2021) 130127.
53. X. Xing, Y. Yang, Z. Yan, Y. Hu, T. Zou, Z. Wang, Y. Wang, *Ceramics International*, 45 (2019) 4322–4334.
54. Y. Sun, Z. Wang, W. Wang, G. Li, P. Li, K. Lian, W. Zhang, S. Zhuiykov, J. Hu, L. Chen, *Materials Research Bulletin*, 109 (2019) 255–264.
55. F. Tian, Y. Liu, K. Guo, *Materials Science in Semiconductor Processing*, 21 (2014) 140–145.
56. X. Wang, S. Zhang, M. Shao, J. Huang, X. Deng, P. Hou, X. Xu, *Sensors and Actuators B: Chemical*, 251 (2017) 27–33.
57. Q. Jia, H. Ji, Y. Zhang, Y. Chen, X. Sun, Z. Jin, *Journal of Hazardous Materials*, 276 (2014) 262–270.
58. C.A. Zito, T.M. Perfecto, T.N.T. Oliveira, D.P. Volanti, *Materials Letters*, 223 (2018) 142–145.